



Noninvasive elemental XRF characterization of mudstone lagerstätten for provenance identification: Advantages and limitations

Alejandro Gil-Delgado, Jordi Ibáñez-Insa, Albert Sellés, Xavier Delclòs, Àngel Galobart, Matías Reolid, David Cruset, Soledad Álvarez, and Oriol Oms

ABSTRACT

The objective of this study is to explore the utility of portable X-ray fluorescence (pXRF) techniques in identifying the geochemical signature of various classical fossil sites within museum collections. The motivation for this research stems from the challenges posed by the Montsec lithographic limestones collection, which has been dispersed globally since the last century. In some cases, tracing the Montsec origin of certain pieces has proven to be unclear. To achieve this goal, we have examined 17 different lagerstätten sites characterized by distinct carbonate lithology and chronology, using various sample sets. The aim is to determine the feasibility of distinguishing each site through pXRF. The results indicate that this goal is achievable in many sites, such as Ockley or Daohugou, where differentiation is clear. However, in some instances, more sensitive XRF instruments or even other non-destructive techniques are required, as seen in the case of Solnhofen site and Montsec lithographic limestones. Nonetheless, even in these cases, some level of differentiation is possible through non-invasive pXRF. Furthermore, within the context of museum collections, we are examining the impact of resin used for fossils conservation (such as Paraloid®-B72) on the detection of compositional signatures. It is noted that resin treatments can bring about changes, such as masking calcium detection and introducing iron into the obtained data.

Alejandro Gil-Delgado. Departament de Geologia, Facultat de Ciències, Universitat Autònoma de Barcelona, Edifici Cs, 08193 - Cerdanyola del Vallès, Catalonia, Spain. alejandro.gil@uab.cat and Museu de la Conca Dellà, Lleida, Spain.

Jordi Ibáñez-Insa. Geosciences Barcelona (GEO3BCN-CSIC), 08028 Barcelona, Catalonia, Spain. jibanez@geo3bcn.csic.es

Albert Sellés. Museu de la Conca Dellà, Lleida, Spain and Institut Català de Paleontologia Miquel Crusafont, 08201, Sabadell, Spain. albert.selles@icp.cat

Final citation: Gil-Delgado, Alejandro, Ibáñez-Insa, Jordi, Sellés, Albert, Delclòs, Xavier, Galobart, Àngel, Reolid, Matías, Cruset, David, Álvarez, Soledad, and Oms, Oriol. 2025. Noninvasive elemental XRF characterization of mudstone lagerstätten for provenance identification: Advantages and limitations. *Palaeontologia Electronica*, 28(1):a3.

<https://doi.org/10.26879/1415>

palaeo-electronica.org/content/2025/5415-xrf-characterization

Copyright: January 2025 Palaeontological Association.

This is an open access article distributed under the terms of the Creative Commons Attribution License, which permits unrestricted use, distribution, and reproduction in any medium, provided the original author and source are credited. creativecommons.org/licenses/by/4.0

Xavier Delclòs. Departament de Dinàmica de la Terra i de l'Oceà, Facultat de Ciències de la Terra, Universitat de Barcelona, 08028, Barcelona, Spain. xdelclos@ub.edu and Institut de Recerca de la Biodiversitat (IRBio), Universitat de Barcelona, 08028, Barcelona, Spain.

Àngel Galobart. Museu de la Conca Dellà, Lleida, Spain and Institut Català de Paleontologia Miquel Crusafont, 08201, Sabadell, Spain. angel.galobart@icp.cat

Matías Reolid. Departamento de Geología, Universidad de Jaén, Campus Las Lagunillas sn, 23071 Jaén, Spain. mreolid@ujaen.es

David Cruset. Geosciences Barcelona (GEO3BCN-CSIC), 08028 Barcelona, Catalonia, Spain. dcruset@geo3bcn.csic.es

Soledad Álvarez. Geosciences Barcelona (GEO3BCN-CSIC), 08028 Barcelona, Catalonia, Spain. salvarez@geo3bcn.csic.es

Oriol Oms. Departament de Geología, Facultat de Ciències, Universitat Autònoma de Barcelona, Edifici Cs, 08193 - Cerdanyola del Vallès, Catalonia, Spain. joseporiol.oms@uab.cat

Keywords: geological heritage; fossil-record; X-ray fluorescence; lithographic limestone; geochemistry

Submission: 2 June 2024. Acceptance: 18 December 2024.

INTRODUCTION

The study of the fossil record provides relevant information about the ecosystems of the past and, therefore, about the history of life on Earth and how it evolved. Unfortunately, the clues provided by fossils are frequently not clear enough due to poor preservation, scarcity of specimens, and/or lack of paleobiological information. Thus, the localization and detailed investigation of the so-called fossil Lagerstätten sites are of paramount importance to achieve significant progress in the field of evolutionary paleontology. The term 'Lagerstätte' is a German word used in sedimentary geology to define any rock body that contains a unique wealth of paleontological information, either in a qualitative or quantitative sense (Seilacher et al., 1985; Behrensmeyer, 2021).

Given the importance of Lagerstätten sites and the invaluable information they provide, many scientific institutions worldwide have been devoted to their thorough investigation since the very birth of the discipline. Examples of well-known classic sites include the famous Upper Jurassic localities of Solnhofen (Bavarian region of Altmühlthal, Germany), Canjuers (Haute Provence, France) or the Cretaceous site of La Pedrera de Meià (southern Pyrenees of Lleida, Spain), among many others of different chronologies and locations around the planet.

Unfortunately, early research on many of these sites was performed before the development of modern collection methodologies. In addition, communication issues among members of international teams were frequent during those times. Thus, although Lagerstätten sites yielded numer-

ous exceptional fossil collections scattered over museums and institutions around the world, there is currently an underlying problem with the classification of many of the available fossils. More recently, some collections have been enriched with samples obtained by amateur collectors and vendors and even after spoliation of the sites, which adds another layer of difficulty to the correct provenance identification of the specimens. In the case of sites with similar lithologies and appearance, such as those composed by carbonate mudstones (as in the case of the sites mentioned above, i.e., Solnhofen, Canjuers and La Pedrera de Meià), the problem is even worse.

It can be hypothesized that the issue of provenance identification could be addressed by analyzing the rock matrix of fossils through geochemical analytical techniques. For example, inductively coupled plasma mass spectrometry (ICP-MS) measurements could offer pertinent compositional information about the major and trace elements of samples composed of carbonate mudstones, which could be complemented with data on the characteristic $\delta^{18}\text{O}$ and $\delta^{13}\text{C}$ isotopic signatures. For instance, the trace elements' quantity in the samples could allow researchers to distinguish samples from different locations. However, ICP-MS and stable isotope analyses would imply the partial destruction of the samples, which is particularly problematic for unique holotypes or specimens with a delicate degree of conservation that cannot be easily subjected to mechanical extraction methods. An ICP-MS study on a large number of samples would be highly expensive and involve a significant bureaucratic burden (and, most likely,

permission to extract material would not be granted by many institutions). In contrast, pXRF provides a much more accessible option due to its cost-effectiveness, operational simplicity, and efficiency compared to ICP-MS or stable isotope techniques, making it a far more practical analytical solution for many institutions.

Portable X-Ray Fluorescence (pXRF) is a fast and powerful analytical tool that provides multielemental data of inorganic materials in a rapid and non-destructive manner. It is widely used in various fields, including applied geochemistry and stratigraphy (Lemière, 2018; Ibáñez-Insa et al., 2017), archaeology and cultural heritage (Madariaga et al., 2016; Biagetti et al., 2021), or environmental research (Rouillon and Taylor, 2016). Since pXRF can be easily employed in museums and institutions to virtually analyze any type of sample and material, it is clear that this technique might provide useful information about the origin of unidentified (or dubious) fossil specimens. In some cases, this technique might even allow one to unambiguously identify the provenance of the samples.

In the present work, we explore the usefulness of pXRF as a fast and non-destructive means to identify the origin of fossil specimens from Lagerstätten sites. For this purpose, pXRF measurements on samples containing fossils from 17

different carbonate mudstone Lagerstätten sites have been performed. The objective of these measurements is to assess, in combination with multivariate statistical methods, whether the multielemental information obtained by pXRF may allow one to constrain, and even identify, the origin of fossil specimens. Our data and analysis suggest that pXRF may provide highly relevant information for this type of provenance studies.

MATERIALS AND METHODS

The main characteristics of each of the 17 sampled Lagerstätten sites (Figure 1) can be found in the Appendix (Table 1). This study is based on the in situ measuring of 37 samples housed in different institutions.

It should be emphasized that La Pedrera de Meià (LPM acronym) fossil site is the ultimate focus of this study. The ongoing research performed in this site laid the groundwork for the present paper by highlighting the need to properly identify the origin of samples that might be dubiously attributed to LPM. This site is in the Montsec range, in the Lleida province (NE Spain). It is part of the formation ‘Lithographic limestones with Plants and Vertebrates of the Pedrera de Rúbies’ (Peybernès and Oertli, 1972), which is included in ‘the Montsec Charophyte Limestone Ensemble’

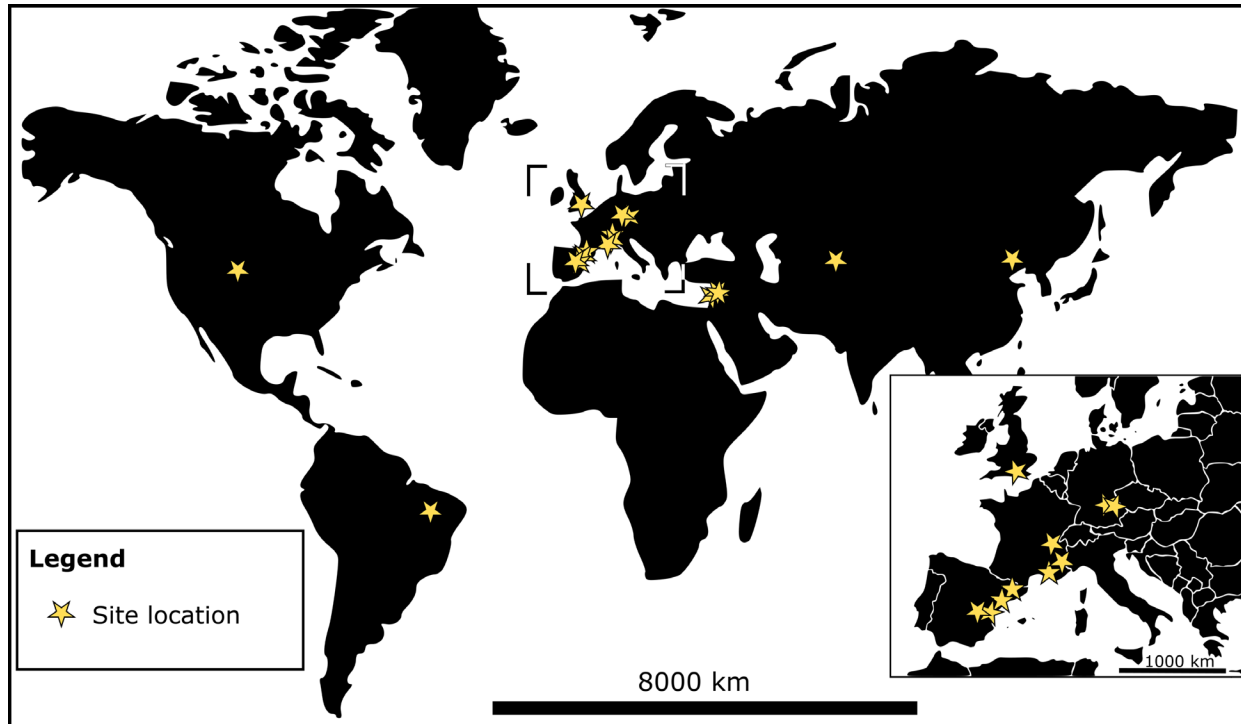


FIGURE 1. Original location of all the studied sites and samples.

(Peybernès, 1976). The lithographic limestones of LPM are dated from the Uppermost Hauterivian to Lower Barremian (around 125.77 My) (Martín-Closas and López-Morón, 1995). Other sites such as La Cabroa site and El Reguer site, among a minimum of four more outcrops of smaller extension (Gil-Delgado et al., 2023a,b), also belong to this unit. These Barremian sites that are the focus of this work are interpreted as the result of a coastal-lake system sedimentation (Barale et al., 1984; Martínez-Delclòs, 1991) within the frame of the Early Cretaceous NE Iberoarmoricane island.

All the other carbonate mudstone sites from around the world included in this study are indicated in the map of Figure 1. In the case of European fossil sites, they are distributed throughout the continent. In the Iberian Peninsula, there are other Lagerstätten sites beyond Montsec: Alcover (Tarragona), Rubielos de Mora (Teruel), and Las Hoyas (Cuenca). Other than those in the Iberian Peninsula, the other European notable sites include Cerin, Canjuers, the Aix-en-Provence site of "Les Plâtrières" (all in France), the Ockley site of Smokejacks Brickworks (UK), and the famous Solnhofen and Kelheim sites, both in Germany. The studied Asian sites include the Lebanese localities of Hakel, Hadjoula, and Sahel Alma; the Karatau site in Kazakhstan; and the Chinese site of Dao-hugou. Finally, samples from the American continent come from the Brazilian Crato Formation and the Wyoming outcrops of the Green River Formation.

The studied samples are housed in the following museums and universities. The lithographic limestones rock samples from LPM were collected during the last paleontological campaigns that began in 2019 and are stored at the Universitat Autònoma de Barcelona stratigraphy department (acronyms R, C and additionally samples from Las Hoyas, LH). On the other hand, the limestone samples from around the world were provided by the curator of the natural collection at the Museu de la Ciència CosmoCaixa (Barcelona), Dr. Alejandro Pérez Jiménez, who granted access to the lithographic fossil pieces (samples acronym as MCFO). Additionally, pieces from the Museu Blau de Barcelona (samples acronym as MGB), and pieces from the Universitat de Barcelona (acronyms Crn, Kr, Mnt-Alc, Ock, RMr, Dhg, Slnh, Crt-Brs and Aix-), were included in this study. The list of the investigated samples with their corresponding reference names can be found in the Appendix Table 1.

Non-destructive pXRF measurements were performed on all the samples investigated in this

work. The measurements on all samples were acquired by using a Bruker Tracer-IV Geo instrument coupled to a tripod (see Figure 2). This analyzer is a portable energy-dispersive (EDS) device that is equipped with a 40 kV rhodium (Rh) X-ray generator and a large area (30 mm^2) silicon drift detector. The size of the analyzed area on the sample is around 8 mm^2 . The instrument is easily controlled through a portable digital assistant (PDA), which allows one to set up the experimental conditions of the analyses and which also displays the quantitative (elemental) data. The measurements were acquired by using one of the internal calibrations set up in the instrument, the so-called "Precious Metals" method as provided by the manufacturer. Typical integration times of 120 s were used. This internal calibration was selected because it allows one to excite and detect XRF signal from the most relevant elements in the limestones, which is achieved by applying high voltages to the X-ray tube. However, in order to analyze the XRF results we did not rely on the semiquantitative data provided by the built-in calibration, since it is clearly not expected to provide reliable results for the limestones. Instead, we extracted the intensity of the observed XRF peaks from the registered spectra (see Ibáñez-Insa et al., 2017 for details). The intensity data thus obtained was normalized to the intensity of the Compton peak. The resulting values can be found in Table 2 of the Appendix. These values enabled us to estimate the relative content, from sample to sample, of different elements, including P, S, Ca, K, Ti, Mn, Fe, Rb, and Sr, among others, and to perform subsequent statistical treatment of the resulting data.

On the other hand, X-Ray micro-fluorescence (μ -XRF) compositional mappings were also obtained from a few samples (Figure 3). The mappings were conducted at Centro de Instrumentación Científico-Técnica CICT (Jaén University, Spain). An energy dispersive X-Ray micro-fluorescence spectrometer was used to map qualitative elemental abundance of samples. Samples were excited using an X-ray tube with a rhodium anode, with a maximum focal spot excitation intensity of 50 kV and 600 μA (30W). The X-ray optics relied on polycapillary tubes which provided an excitation point of up to 25 μm . This allowed to focus the beam on a restricted area of the sample, covering a measurement range from Na to U. The fluorescence that was emitted by the sample was collected by an energy dispersive detector having an active area of 30 mm^2 . These measurements allowed us to visualize the spatial distribution of dif-

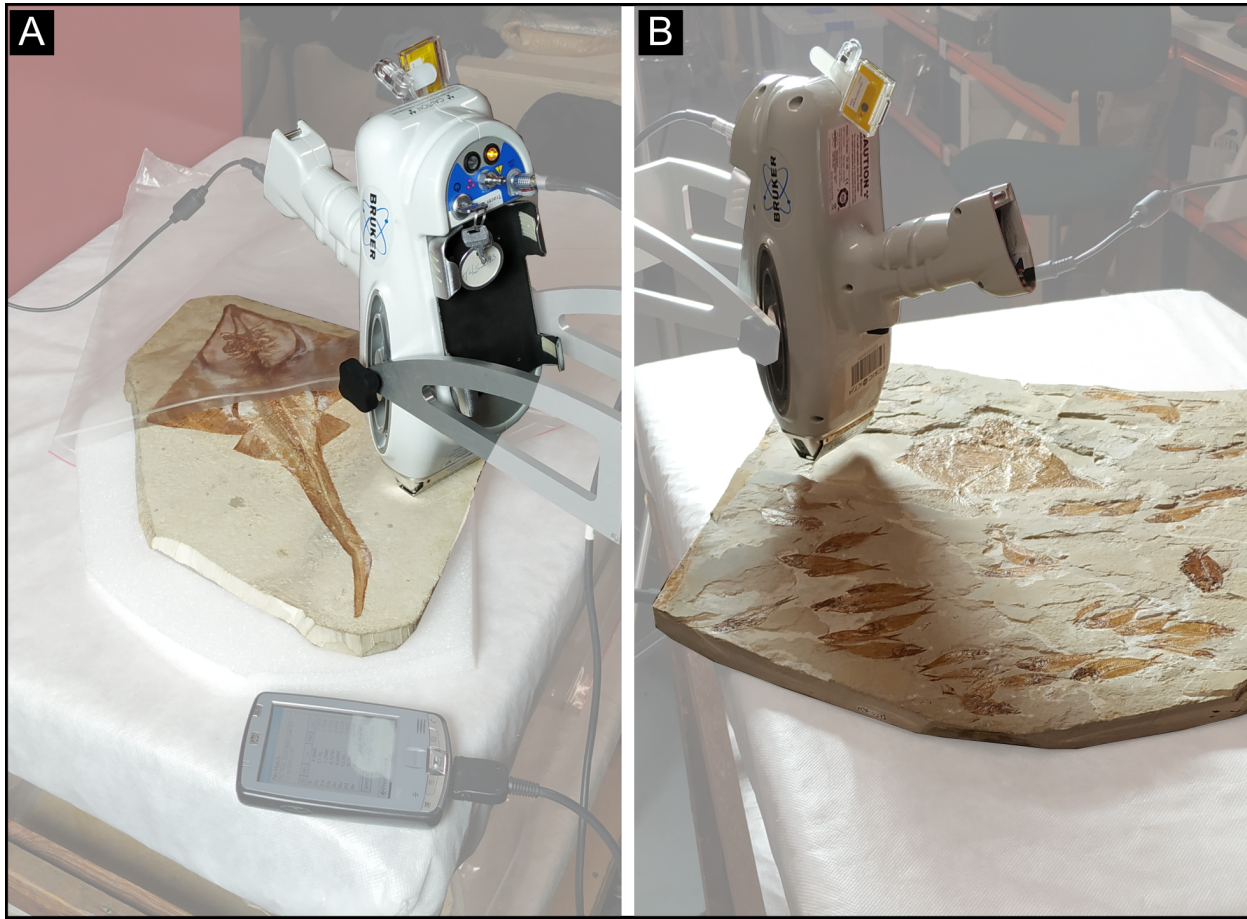


FIGURE 2. Sampling of the Museu de la Ciència CosmoCaixa natural collection with portable XRF. A) Sampling of Hakel (Lebanon) Cretaceous site, within a *Rhinobatos* sp. (MCFO-0521). B) Sampling of Hjoula (Lebanon) Cretaceous site, within fossils of Beryciformes fishes, Picnodontiformes, *Armigatus* sp. and *Triplomystus* sp. (MCFO-0372).

ferent chemical elements within the investigated samples at the submicrometric scale, which enabled us to better understand the type of information that can be gained from the fossils themselves or from their surrounding rock matrices.

RESULTS AND DISCUSSION

It should be first emphasized that strong compositional variations within a single specimen or among samples from the same site would imply that the XRF technique is not reliable for a provenance study. Therefore, and as an initial step, we obtained μ -XRF mappings from a few fossil samples of a single site (LPM) in order to assess their compositional homogeneity. Figure 3 shows selected μ -XRF mappings for several elements (Ca, K, P, S, Ti) from two different samples from LPM. As expected, the fossils exhibit particular elemental enrichments depending on the type of fossil (plant or animal) and the type of preserved tissue.

In the case of plant remnants (upper panels), elements like S and also Ti are clearly enriched relative to the surrounding rock and also to other fossils. In contrast, the P content is significantly enhanced in the case of the animal fossil (bottom panel). Given the multifaceted biological functions of P and its pivotal role in skeletal mineralization (Michigami and Ozono, 2019), the observation of heightened concentrations of this element associated with such structures in MCD-7163 is unsurprising. Alongside Ca, P serves as the primary structural mineral component of fish bones, predominantly comprising hydroxyapatite ($\text{Ca}_{10}[\text{PO}_4]_6[\text{OH}]_2$) (Toppe et al., 2007). Previous works in μ -XRF concludes that metabolism-related vital effects prominently influence the co-precipitation and adsorption of trace elements in animal skeletal parts, particularly for Ca, Mg, Sr, Ba, and Zn. What is more, environmental parameters, including salinity and temperature across various water depths, have to be correlated to rates and

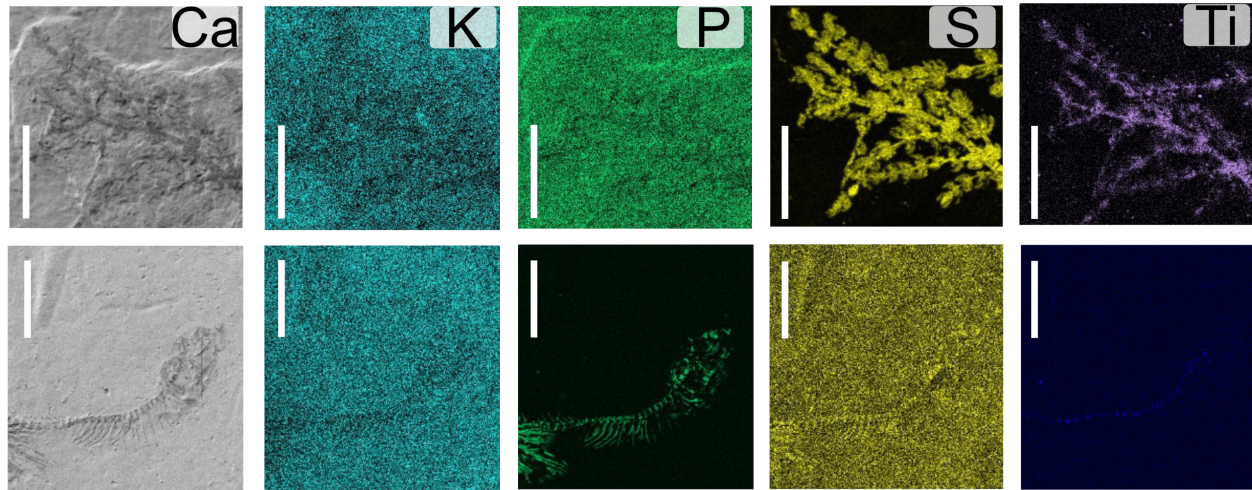


FIGURE 3. Compositional mapping with micro-XRF for different elements. The upper panels correspond to plant MCD-8492 (*Montsechia vidalii*) and the lower panels to teleostean fish MCD-7163 from the Museu de la Conca Dellà collection. The intensity of color indicates a qualitative measure of abundance for each individual element. Scale bar equals 5 mm.

trace elements incorporation in different parts of the taxa (Reolid et al., 2023).

In contrast, K is depleted in both specimens, while trace elements like Cr (not shown) seem to be slightly enriched in both fossils relative to the matrix. The latter might be related to the fact that organic matter may have acted as a redox trap during fluid circulation in early diagenetic stages. In the case of Ca, both fossils seem to be partially depleted in this element. In contrast, it is seen that the rock matrix is highly homogenous in both specimens, thus suggesting that only the rock matrix, not the fossils, is sufficiently homogeneous in order to perform the present exploratory provenance study. To put it in another way, only the rock matrix has potential to be an XRF ‘fingerprinting’ of the sample provenance.

Figure 4 shows selected XRF spectra for the particular case of samples from three different locations: LPM, Solnhofen, and Haquel. These particular spectra were excited with high voltage conditions in order to preferentially excite heavier elements (atomic numbers $Z > Fe$). Similar spectra excited with low voltages were also obtained in order to excite lighter elements ($Z < Fe$). In spite of the high voltage to obtain the experimental results of Figure 4, all the spectra are dominated by a strong signal from Ca ($K\alpha$ and $K\beta$ peaks) around 4 keV, which is a consequence of the calcareous composition of all the analyzed samples. In the region around 20 keV, peaks from coherent and incoherent scattering (Rayleigh and Compton peaks) are also observed. In addition, weaker

peaks from other elements like K, Ti, Mn, Fe, Rb, and Sr also show up with different intensities in the three spectra. Many of these elements may be attributed to a clastic origin (for instance, K, Ti, Rb, and Fe), while others may reflect the particular geochemical conditions of the deposit (Sr). Note that other much weaker peaks are also detected in some spectra for trace elements like Cr, Cu, or Zn. However, such features are very close to the detection limit of the technique and, as a consequence, will not be considered here.

Interestingly, the sample from Haquel (Figure 4) seems to contain higher amounts of K, Ti, Rb, or Fe, which might imply a larger amount of detrital input in this site. In contrast, the XRF spectra shown in Figure 4 for the Solnhofen and LPM samples are very similar. These spectra suggest that samples of Haquel might be easily distinguished from specimens of Solnhofen and LPM. In contrast, the compositional similarity of these two sites as highlighted in the spectra of Figure 4 seem to suggest that pXRF might not be a useful tool to distinguish samples from these two deposits. It should be emphasized that very similar results are found for the rest of samples from these three locations that have been included in the present study. In other words, the samples from a given site seem to be sufficiently similar from a compositional point of view, making the pXRF technique fairly promising to quickly evaluate the provenance of fossil specimens from Lagerstätten sites, at least in some specific cases. Table 2 in the Appendix shows the intensity values for each detected element as

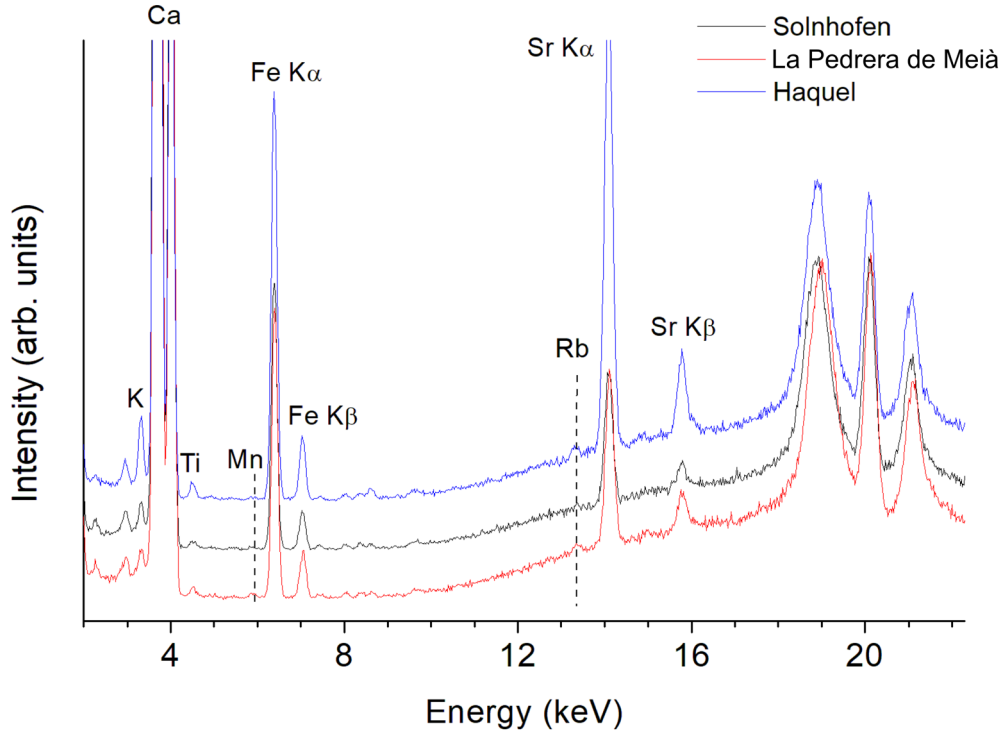


FIGURE 4. Selection of X-ray fluorescence spectra of three samples studied in this work (Solnhofen, Pedrera de Meià, and Haquel). The results obtained for other samples are in general similar to those plotted in the figure. In all cases, the spectra are dominated by strong Ca alpha and Ca beta peaks around 4 keV. In addition, other features arising from minor elements in the limestone samples show up in the spectra (K, Fe, Rb, Sr, etc.). Remarkably, the XRF spectra from Solnhofen and LPM (black and red curves, respectively) are very close to each other, with only minor intensity variations among peaks. In contrast, the spectrum from Haquel (blue curve) shows increased signal for many of the detected elements (K, Fe, Ti). This observation suggests that Haquel samples tend to display larger amounts of elements like K, Fe, and Ti, which can be attributed to a detrital origin. The similarity between Solnhofen and LPM limestones might indicate similar depositional conditions in these two sites.

obtained from full-profile fitting of all the pXRF spectra obtained in this work.

It should be noted that the juxtaposition of XRF spectra for samples of different sites, as in Figure 4, or even the direct comparison of the intensity values displayed in Appendix Table 2, allows us to identify a recurring feature in all the samples, namely, the fingerprinting ability of the Sr and the Fe K α peaks alone. This characteristic enables one to distinguish between samples that, for the particular experimental conditions of the present measurements, display Fe peaks that are more intense than those of Sr (Ockley, Montsec sites, Daohugou, Haute-Provence, Solnhofen, Kelheim, Monreal-Alcover, and Rubielos de Mora), and those exhibiting a more intense Sr peak (Crato, Lebanon, Aix-en-Provence, Las Hoyas, Karatau, Cerin, Haquel, and Green River). This is depicted in Figure 5, which shows the intensity of the Sr and

Fe peaks as obtained from all the present measurements. The figure shows that most of the analyzed samples exhibit relatively low Fe signal, with varying amounts of Sr.

It is interesting to note that the intensity of the Fe and Sr peaks in the Bavarian sites and the Montsec lithographic limestones, despite differing in age, genesis, and geographical location, is found to be very similar. Together with the samples from Cerin, the materials from Montsec and Solnhofen display the lowest Fe and Sr signals. This is in contrast to the samples of Las Hoyas which, in spite of sharing a similar lithology, age and maybe even depositional conditions to those from Montsec and Solnhofen, are found to contain significantly larger amounts of Sr (see Figure 5).

For comparison, Figure 6 shows the intensity of K and Ca peaks from all the samples investigated in this work. As can be seen in the plot,

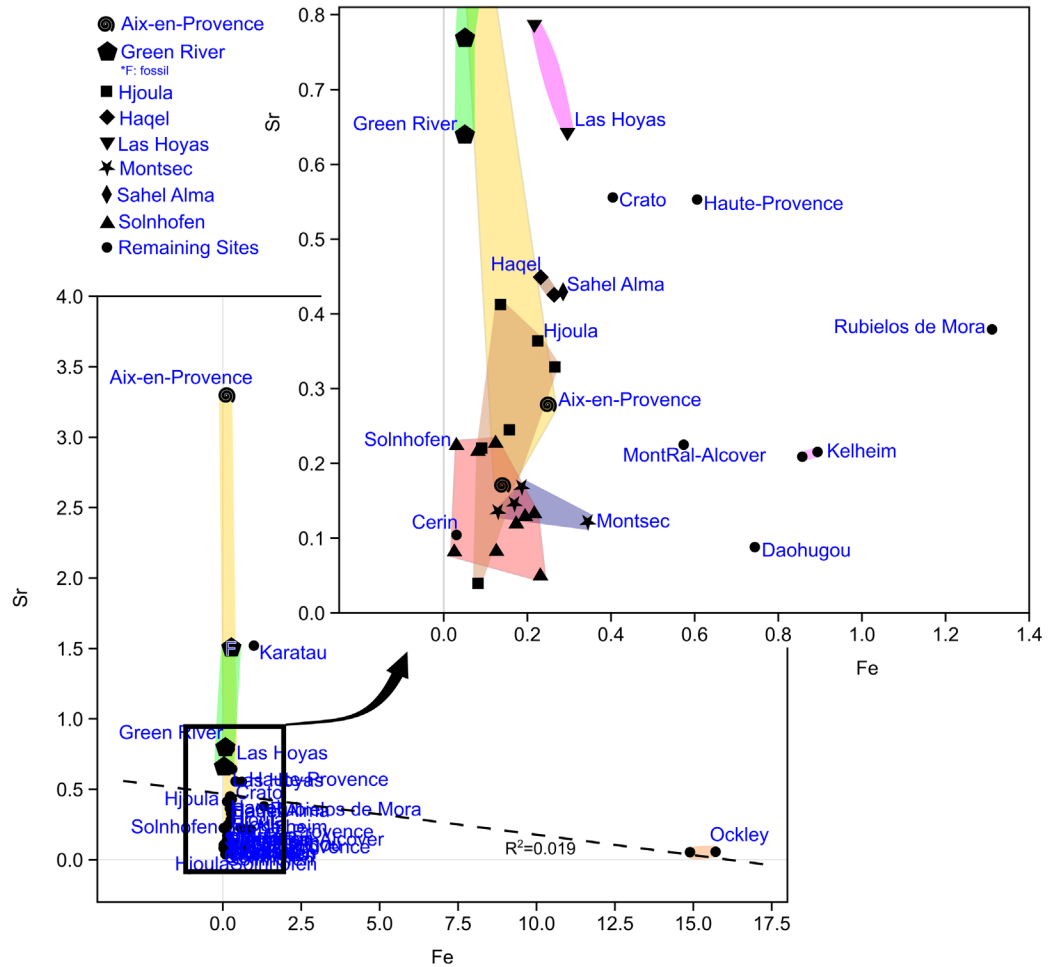


FIGURE 5. Plot of the intensity of the Fe and Sr peaks, as extracted from the XRF spectra (see text) for all the samples analyzed in the present work.

many of the samples cluster around a Ca-rich area, while the rest seem to exhibit lower amounts of Ca that might be tentatively linked to materials with higher amounts of impurities like, for instance, detrital inputs. However, as shown in Figure 6, the anticorrelation between the intensity of Ca and K peaks is very weak and, therefore, other factors like porosity might be affecting the overall intensity of the Ca peak in all these samples. It should be noted that, on the other hand, the XRF signal of Ca in the Solnhofen samples exhibits large variability, with two particular samples displaying much lower Ca intensities than the rest. A similar behavior can be found in samples from Hjoula, most of which nicely cluster in the Ca-K plot with the exception of one specimen, which exhibits much lower Ca intensity.

It is clear from Figures 5 and 6 that the XRF signals are partly determined by the provenance of

the samples, although with limited ability for discrimination purposes. This is further reflected in the principal component analysis (PCA), plotted in the bottom left part of Figure 7, performed with the data of Table 2 of the Appendix. In this case, the first principal component (PC1) explains around 58% of the variance, while the second component (PC2) explains around 17% of the variance. The figure shows how dimensionality reduction leads to a separation of the samples in different groups: Sr-rich samples (Karatau and Aix-en-Provence), Fe and K-rich samples (Rubielos de Mora, Daohugou and Ockley), and the rest of samples, which are Ca-rich. The zoom to the PCA plot for these samples (top right of Figure 7) shows how samples from the same origin tend to cluster together. As can be seen in the plot, samples from Montsec and Solnhofen exhibit very similar values of PC1 and PC2 and, as already suggested in the above dis-

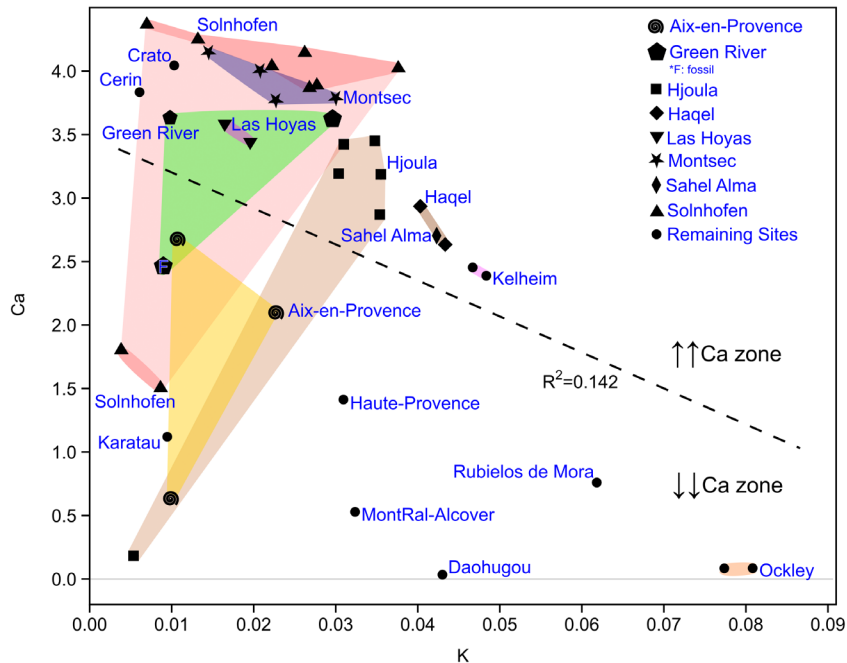


FIGURE 6. Plot of the intensity of the K and Ca peaks, as extracted from the XRF spectra (see text) for all the samples analyzed in the present work.

cussion, samples from these sites do not seem to be distinguishable by XRF alone. In the case of samples from other sites, however, the present data suggest that, at least for a preliminary provenance characterization, portable XRF instruments may be of help.

The present study has shown the potential, but also some of the limitations, of pXRF in order to assess the provenance of fossil specimens. We have seen that the compositional similarity of different sites may restrict the applicability of the technique. An additional limitation may be introduced by the resins employed in museum collections to protect the specimens, as these materials may significantly affect the XRF results. To further investigate this, we have conducted several tests to examine the effects of a commonly used resin, Paraloid®-B72, on the XRF spectra. For this purpose, we have measured different XRF on limestones from Montsec that had been previously treated with Paraloid®-B72 with 0%, 5%, and 10% concentrations, using acetone as the solvent. The resulting XRF spectra are shown in Figure 8. As can be seen in the figure, plotted with a logarithmic scale, the resin has a bearing on the lighter elements, including Ca. In contrast, the XRF signal from heavier elements like Sr is basically unaltered. These observations can be attributed to absorption of the lower-energy X-rays from the

lighter elements by the organic resin. Note, however, that there is no a proportional behavior between Paraloid®-B72 composition and the XRF intensities, which might be related to the variable thickness of the applied treatments and also to the presence of impurities in the organic compounds. In any case, it is clear that decreased amounts of Fe, Ca, or K might be detected in samples with sufficiently thick films of Paraloid®-B72, thus altering any subsequent provenance analysis. In the case of this study, the presence of the resin might explain the observation of samples from Solnhofen with particularly low Ca contents. However, it cannot be ruled out that some of the studied specimens were not correctly attributed. Therefore, additional work should be performed in order to assess the presence of resin treatments in fossil specimens and their effect on the XRF signals.

Finally, it would be highly interesting to investigate whether a combination of pXRF with other non-destructive techniques, such as magnetic susceptibility measurements, hyperspectral imaging methods, or machine learning algorithms, could improve the discrimination of fossil specimen provenance. Additionally, the Laser-Stimulated Fluorescence (LSF) technique, which can rapidly produce qualitative geochemical images of sedimentary rocks with ppm sensitivity (Kaye et al. 2015), presents a promising future avenue. An LSF study of

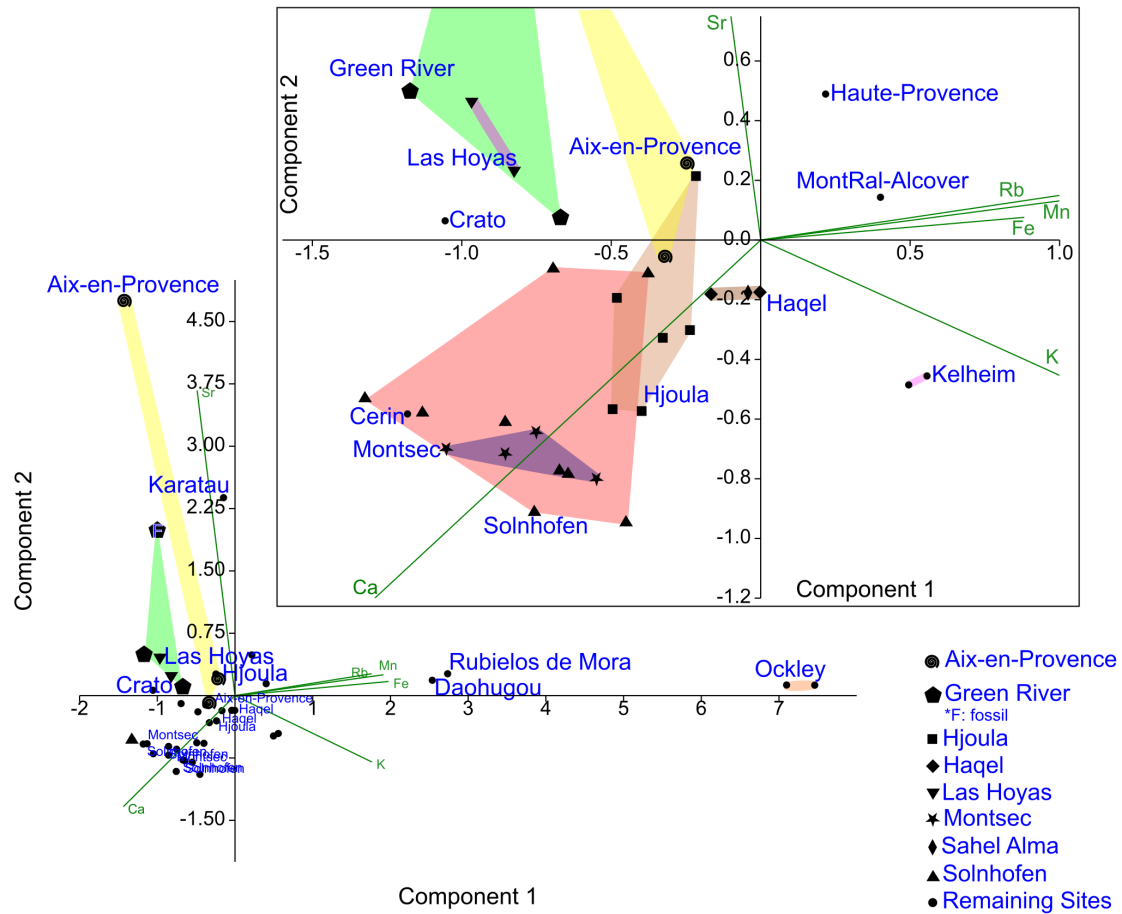


FIGURE 7. Principal Component analysis of the studied samples. Framed plot is the enlargement of the smaller values of each component.

our samples could potentially allow for extrapolation of analytical point data across larger sample areas and suggest additional fluorescence points for measurement (Pittman et al., 2022), making it a valuable direction for further exploration. Furthermore, it is important to note that in this exploratory study, the compositional variability within each site is often underrepresented by one or a few samples, meaning that many more analyses would be needed to establish a comprehensive and complete compositional data-set for future provenance studies.

CONCLUSIONS

The XRF data analysis, Principal Component Analysis (PCA), and statistical techniques has proven indispensable in elucidating the elemental composition of diverse fossil sites globally. The non-destructive nature of XRF adds a significant dimension to this exploration, allowing for comprehensive data acquisition without compromising the

integrity of valuable samples. Noteworthy patterns, dominated by elements such as Fe, Sr, Rb, and K, emphasizing the utility of the XRF technique in revealing elemental characteristics.

The differentiation between sites, as revealed through PCA plots, often corresponds to specific geological factors, highlighting the impact of genesis and local diagenetic processes. The study encompasses a diverse range of fossil sites than Montsec lithographic limestones, including Montral-Alcover, Rubielos de Mora, Las Hoyas, Karatau, Daohugou, Green River, Crato, Kelheim, and Solnhofen, each presenting a diagnostic elemental data-set shaped by lithology, composition, and environmental conditions.

A crucial aspect of this research lies in recognizing the potential impact of resin alteration, specifically the masking potential of Paraloid®-B72, on compositional results in museum collections. Caution is advised in interpreting XRF data from resin-

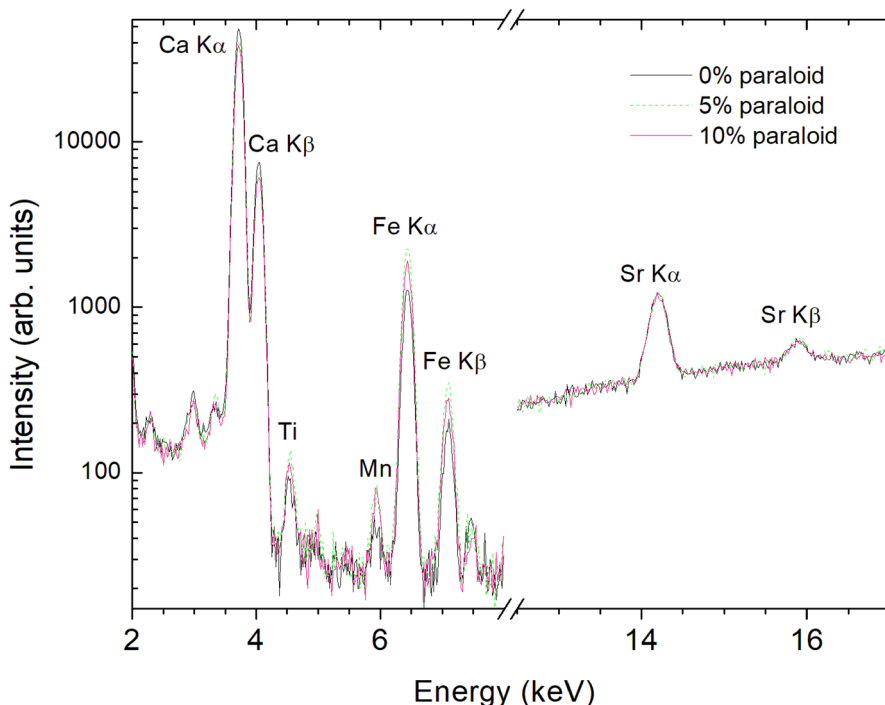


FIGURE 8. X-ray fluorescence spectra from samples from LPM treated with different concentrations of Paraloid®-B72. Note the logarithmic scale.

treated samples, emphasizing the need for meticulous consideration in subsequent analyses.

Looking forward, the study advocates for the utilization of more sensitive XRF machines, offering a glimpse into the potential to assign pieces to specific outcrops based on their rock matrix fluorescence chemical signature. This non-destructive approach aligns with the principles of preserving invaluable collections while advancing traceability and origin determination in paleontological research. Notably, the ability of XRF to produce results akin to those obtained by the destructive ICP-MS method underscores its efficacy and further positions XRF as a valuable tool in the comprehensive analysis of fossils. In conclusion, the integration of advanced analytical techniques and the non-destructive capabilities of XRF contribute to a nuanced understanding of elemental characteristics in paleontological sites studies.

ACKNOWLEDGEMENTS

This work has been funded by Spanish Government MCIN project PGC2018-101575-B-I00. “Dynamics of transitional settings from Cretaceous to Eocene in the south-central Pyrenees”; and the Generalitat de Catalunya (CERCA Program); and project Characterization of transgressive mixed

sedimentary successions from the southern Pyrenees: paleoenvironmental and reservoir implications (PID2023-151769NB-I00). AGD was supported by the AGAUR program for the doctoral formation grant 2020 FI SDUR 00360. MR research is supported by RNM-200 research group of the Junta de Andalucía and research project PID2019-105537RB-100 of the Spanish Government, Ministry of Economy and Competitiveness. ASG research is supported by the project VIGOCULT (PLEC2021-00793) funded by MCIN/AEI/10.13039/501100011033 and by the European Union NextGenerationEU/PRTR. ASG and AG acknowledges the project ARQ001SOL-173-2022 (“El Cretaci continental del Pirineu meridional català: ecosistemes i evolució faunística. 2022-2025”) funded by the Departament de Cultura of the Generalitat de Catalunya and the CERCA Program. We are grateful to Orígens UNESCO Global Geopark for facilitating fieldwork in the Montsec area. This work is part of AGD’s PhD thesis, conducted within the framework of a doctoral program in Geology at UAB. OO belongs to research group 2021SGR 00127. Finally, we express our gratitude to Dr. A. Pérez Jiménez for granting us access to the CosmoCaixa fossil collection, and to Dra. Y. Díaz Acha for providing us with pieces from the

Museu de Ciències Naturals de Barcelona. The constructive and detailed review comments from Dr. M. Pittman, an anonymous reviewer, and from

handling editor Dr. R.N. Felice have contributed to sharpening the manuscript and are gratefully acknowledged.

REFERENCES

- Anadón, P. 1983. Características generales de diversas cuencas lacustres terciarias con pizarras bituminosas del NE de la Península Ibérica. Comunicaciones del X Congreso Nacional de Sedimentología, Menorca, 1:9–12.
- Anadón, P., Cabrera, L., Inglés, M., Julia, R., and Marzo, M. 1988. The Miocene lacustrine basin of Rubielos de Mora, Excursion Guidebook. International workshop-field seminar on lacustrine facies models in rift systems and related natural resources. Barcelona-Rubielos de Mora.
- Arai, M. and Assine, M.L. 2020. Chronostratigraphic constrains and paleoenvironmental interpretation of the Romualdo Formation (Santana Group, Araripe Basin, Northeastern Brazil) based on palyontology. Cretaceous Research, 116:104610. <https://doi.org/10.1016/j.cretres.2020.104610>
- Bailleul, A., Ségalen, L., Buscalioni, A.D., Cambra-Moo, O., and Cubo, J. 2011. Palaeohistology and preservation of tetrapods from Las Hoyas (Lower Cretaceous, Spain). Comptes Rendus Paleovol, 10:367–380. <https://doi.org/10.1016/j.crpv.2011.05.002>
- Barale, G., Blanc-Louvel, C., Buffetaut, E., Courtinat, B., Peybernes, B., Boada, L.V., and Wenz, S. 1984. Les gisements de calcaires lithographiques du Crétacé inférieur du Montsech (Province de Lérida, Espagne). Considerations paléoécologiques. Geobios. Mémoire spécial 8:275–283. [https://doi.org/10.1016/S0016-6995\(84\)80182-5](https://doi.org/10.1016/S0016-6995(84)80182-5)
- Barrios-de Pedro, S., Poyato-Ariza, F.J., Moratalla, J.J., and Buscalioni, A.D. 2018. Exceptional coprolite association from the Early Cretaceous continental Lagerstätte of Las Hoyas, Cuenca, Spain. PLoS ONE, 13(5):e0196982. <https://doi.org/10.1371/journal.pone.0196982>
- Behrensmeyer, A.K. 2021. Taphonomy, p. 12–22. In Alderton, D. and Scott A.E. (eds.), Encyclopedia of Geology (Second Edition), Academic Press.
- Bernier, P., Gaillard, C., Barale, G., Bourseau, J.P., Buffeteau, E., Gall, J.C., and Wenz, S. 1994. The underlying substrate of the Cerin lithographic limestone. [Le substratum des calcaires de Cerin (Ain, France).] Geobios M.S., 16:13–24. [https://doi.org/10.1016/S0016-6995\(94\)80017-0](https://doi.org/10.1016/S0016-6995(94)80017-0)
- Biagetti, S., Alcaina-Mateos, J., Ruiz-Giralt, A., Lancelotti, C., Groenewald, P., Ibañez-Insa, J., Gur-Arie, S., Morton, F., and Merlo, S. 2021. Identifying anthropogenic features at Seoke (Botswana) using pXRF: Expanding the record of southern African Stone Walled Sites. Plos One, 16(5):e0250776. <https://doi.org/10.1371/journal.pone.0250776>
- Briggs, D.E.G., Pérez-Moreno, B.P., Sanz, J.L., and Fregenal-Martínez, M. 1997. The mineralization of dinosaur soft-tissue in the Lower Cretaceous of Las Hoyas, Spain. Journal of the Geological Society of London, 154:587–588. <https://doi.org/10.1144/gsjgs.154.4.0587>
- Brito Neves, B.B., Santos, E.J., and Van Schmus, W.R. 2000. Tectonic history of the Borborema Province, Northeastern Brazil, p. 151–182. In Cordani, U.G., Milani, E.J., Thomaz Filho, A., and Campos, D.A. (eds.), Tectonic Evolution of South America. 31st International Geological Congress. Rio de Janeiro: Instituto de Geociências, Universidade de São Paulo.
- Calvet, F. and Tucker, M.E. 1995. Geological setting Alcover laminated dolomites, p. 73–79. In Martínez-Delclòs X. (ed.), Montsec and Monreal-Alcover. Two Konservat-Lagerstätten, Catalonia, Spain. II International Symposium on Lithographic Limestones Field Trip Book. Institut d'Estudis Ilerdencs, Lleida.

- Dias, J.J. and Carvalho, I.S. 2022. The role of microbial mats in the exquisite preservation of Aptian insect fossils from Crato Lagerstätte, Brazil. *Cretaceous Research*, 130:105068. <https://doi.org/10.1016/j.cretres.2021.105068>
- Doludenko, M.P. and Orlovskaya, E.R. 1976. Jurassic floras of the Karatau Range, southern Kazakhstan. *Palaeontology*, 19:627–640.
- Doludenko, M.P., Sakulina, G.V., and Ponomarenko, A.G. 1990. The geology and Late Jurassic fauna and flora of a unique locality of Aulie (Karatau Mountains, southern Kazakhstan). Moscow Geologicheskii Institut, Akademii Nauk SSSR:38.
- Ejel, F. and Dubertret, L. 1966. Sur l'âge précis du gisement de poissons et de crustacés de Sahel Alma (Liban). *Compte Rendu Sommaire des Séances de la Société Géologique de France*, 6:353.
- Ferry, S., Merran, Y., Grosheny, D., and Mroueh, M. 2007. The Cretaceous of Lebanon in the Middle East (levant) context. *Carnets de Géologie, Mémoire* 2(8):38–42. <https://hal.science/hal-00166894>
- Forey, P.L., Yi, L., Patterson, C., and Davies, C.E. 2003. Fossil fishes from the Cenomanian (Upper Cretaceous) of Namoura, Lebanon. *Journal of Systematic Palaeontology*, 1:227–330. <https://doi.org/10.1017/S147720190300107X>
- Fregenal, M.A. and Meléndez, N. 1992. Alta resolución paleoambiental de secuencias lacustres en relación con su potencial de preservación de biotas fósiles. Dos ejemplos del Cretácico Inferior de la Península Ibérica: yacimientos de Las Hoyas (Cuenca) y de la Sierra del Montsec (Lleida), España. III Congreso Geológico de España y VIII Congreso Latinoamericano de Geología. Salamanca. Simposios tomo 1:70–77.
- Fregenal-Martínez, M.A. and Meléndez, N. 2016. Environmental reconstruction: a historical review, p. 14–28. In Poyato-Ariza F.J. and Buscalioni A.D. (eds.). *Las Hoyas: A Cretaceous wetland. A multidisciplinary synthesis after 25 years of research on an exceptional fossil Lagerstätte from Spain*. Dr. Friedrich Pfeil Verlag. München, Germany.
- Galobart, À., Párraga, J., Gil-Delgado, A. 2022. The Spread of Fossil heritage: How to Valorise the Lithographic Limestones of the La Pedrera de Meià and La Cabroa Quarries in the Orígens Unesco Global Geopark (Southern Pyrenees, Catalonia). *Geoheritage* 14:34. <https://doi.org/10.1007/s12371-022-00669-w>
- Gaudant, J., Nel, A., Nury, D., Véran, M., and Carnevale, G. 2017. The uppermost Oligocene of Aix-en-Provence (Bouches-du-Rhône, Southern France): A Cenozoic brackish subtropical Konservat-Lagerstätte, with fishes, insects and plants. *Comptes Rendus Palevol*, 17(7): S1631068317300799. <https://doi.org/10.1016/j.crpv.2017.08.002>
- Gil-Delgado, A., Delclòs, X., Sellés, A., Galobart, A., and Oms, O. 2023a. The Early Cretaceous coastal lake Konservat-Lagerstätte of La Pedrera de Meià (Southern Pyrenees). *Geologica Acta*, 21(3):1–18, I–XIII. <https://doi.org/10.1344/GeologicaActa2023.21.3>
- Gil-Delgado, A., Cruset, D., Oms, O., Botero, E., Ibáñez-Insa, J., Delclòs, X., Sellés, A., Galobarte, A., and Mercedes-Martín, R. 2023b. Geochemical approach for decoding the paleoenvironmental and depositional evolution of a coastal lacustrine Konservat-Lagerstätte (Early Cretaceous, south-Central Pyrenees). *Sedimentary Geology*, 453:106440. <https://doi.org/10.1016/j.sedgeo.2023.106440>
- Grande, L. 1984. Paleontology of the Green River Formation, with a review of the fish fauna. Geological Survey of Wyoming. Vol. 63. Laramie, Wyoming.
- Gupta, N.S., Cambra-Moo, O., Briggs, D.E.G., Love, G.D., Frenegal-Martinez, M.A., and Summons, R.E. 2008. Molecular taphonomy of macrofossils from the Cretaceous of Las Hoyas Formation, Spain. *Cretaceous Research*, 29:1–8. <https://doi.org/10.1016/j.cretres.2006.12.009>
- Ibáñez-Insa, J., Pérez-Cano, J., Fondevilla, V., Oms, O., Rejas, M., Fernández-Turiel, J.L., and Anadón, P. 2017. Portable X-ray fluorescence identification of the Cretaceous–Paleogene boundary: Application to the Agost and Caravaca sections, SE Spain. *Cretaceous Research*, 78:139–148. <https://doi.org/10.1016/j.cretres.2017.06.004>
- Jattiot, R., Brayard, A., Fara, E., and Charbonnier, S. 2015. Gladius-bearing coleoids from the Upper Cretaceous Lebanese Lagerstätten: diversity, morphology, and phylogenetic implications. *Journal of Paleontology*, 89(1):148–167. <https://doi.org/10.1017/jpa.2014.13>

- Kaye, T.G., Falk, A.R., Pittman M., Sereno, P.C., Martin, L.D., Burnham, David A., Gong, Enpu, Xu,Xing, and Wang, Yinan. 2015. Laser-Stimulated Fluorescence in Paleontology. PLOS ONE 10(5): e0125923:
<https://doi.org/10.1371/journal.pone.0125923>
- Keupp, H., Koch, R., Schweigert, G., and Viohl, G. 2007. Geological history of the Southern Franconian Alb – the area of the Solnhofen Lithographic Limestone. Neues Jahrbuch für Mineralogie, Geologie, und Paläontologie. Abhandlungen, 245:3–21.
<https://doi.org/10.1127/0077-7749/2007/0245-0003>
- Lemiere, B. 2018. A review of pXRF (field portable X-ray fluorescence) applications for applied geochemistry. Journal of Geochemical Exploration, 188:350–363.
<https://doi.org/10.1016/j.gexplo.2018.02.006>
- Liu, Q., Khramov, A.V., Zhang, H., and Jarzembowksi, E.A. 2015. Two new species of *Kalligrammula* Handlirsch, 1919 (Insecta, Neuroptera, Kalligrammatidae) from the Jurassic of China and Kazakhstan. Journal of Paleontology, 89(3):405–410.
<https://doi.org/10.1017/jpa.2015.25>
- Lundberg, J.G. and Case, G.R. 1970. A new catfish from the Eocene Green River Formation. Journal of Paleontology, 44(3):451–457.
- Madariaga, J.M., Maguregui, M., Castro, K., Knuutinen, U., and Martínez-Arkarazo, I. 2016. Portable Raman, DRIFTS, and XRF analysis to diagnose the conservation state of two wall painting panels from Pompeii deposited in the Naples National Archaeological Museum (Italy). Applied Spectroscopy, 70(1):137–146.
<https://doi.org/10.1177/0003702815616589>
- Martín-Closas, C., López-Morón, N. 1995. The charophyte flora, p. 29–31. In Delclòs, X. (ed.), Montsec and Monreal-Alcover. Two Konservat Lagerstätten, Catalonia, Spain. II International Symposium on Lithographic Limestones Field Trip Book Lleida, Institut d'Estudis Ilerdencs, Lleida.
- Martínez-Delclòs, X. 1991. Les calcàries litogràfiques del Cretaci inferior del Montsec. Deu anys de campanyes paleontològiques. Institut d'Estudis Ilerdencs, Lleida.
- Meister, C. 1993. Les collections du département de géologie et de paléontologie du Musée d'Histoire Naturelle de Genève, La collection des poissons du Liban. Revue de Paléobiologie, 12:301–310.
- Michigami, T. and Ozono, K. 2019. Roles of phosphate in skeleton. Frontiers in Endocrinology, 10:180.
<https://doi.org/10.3389/fendo.2019.00180>
- Moissenet, E. and Gautier, F. 1971. La région de Rubielos de Mora (Province de Teruel, Chaines Ibériques orientales). Contribution à l'étude géologique et morphologique. Mélanges de la Casa de Vélezquez, 7:5–28.
- Peybernès, B. 1976. Le Jurassique et le Crétacé inférieur des Pyrénées franco-espagnoles entre la Garonne et la Méditerranée, (Doctoral dissertation), C.R.D.P. Toulouse, France.
- Peybernès, B. and Oertli, H. 1972. La série de passage du Jurassique au Crétacé dans le Bassin sud-pyrénéen (Espagne). Comptes Rendus de l'Academie des Sciences, 274:3348–3351.
- Peyer, K., Charbonnier, S., Allain, R., Läng, É., and Vacant, R. 2014. A new look at the Late Jurassic Canjuers conservation lagerstätte (Tithonian, Var, France). Comptes Rendus Palevol 13:403–420.
<https://doi.org/10.1016/j.crpv.2014.01.007>
- Pittman, M., Kaye, T.G., Graham, E., and Thorold, D. 2022. Laser-stimulated fluorescence in archaeology: non-destructive fluorescence imaging for museum and field settings. Journal of Archaeological Science: Reports. 44:103475
- Ponomarenko, A.G. and Ren, D. 2010. First record of *Notocupes* (Coleoptera: Cupedidae) in the locality of Daohugou, Middle Jurassic of Inner Mongolia, China. Annales Zoologici, 60:169–171.
<https://doi.org/10.3161/000345410X516812>
- Poyato-Ariza F.J. and Buscalioni A.D. 2016. Las Hoyas: A Cretaceous wetland. A multidisciplinary synthesis after 25 years of research on an exceptional fossil Lagerstätte from Spain. Dr. Friedrich Pfeil Verlag, München, Germany.
- Rasnitsyn, A.P. and Zhang, H.C. 2004. Composition and age of the Daohugou hymenopteran assemblage from Inner Mongolia, China. Palaeontology, 47:1507–1517.
<https://doi.org/10.1111/j.0031-0239.2004.00416.x>

- Reolid, M., Reolid, J., Betzler, C., and Lindhorst, S. 2023. Chemical fractionation in benthic fauna from Saya de Malha Bank (Mascarene Plateau, western Indian Ocean): Vital and habitat effects. *Continental Shelf Research*, 266:105078.
<https://doi.org/10.1016/j.csr.2023.105078>
- Ribeiro, A.C., Ribeiro, G.C., Varejao, F.G., Battirola, L.D., Pessoa, E.M., Simoes, M.G., Warren, L.V., Riccomini, C., and Pojato-Ariza, F.J. 2021. Towards an actualistic view of the Crato Konservat-Lagerstatte paleoenvironment: A new hypothesis as an Early Cretaceous (Aptian) equatorial and semi-arid wetland. *Earth-Science Reviews*, 216:103573.
<https://doi.org/10.1016/j.earscirev.2021.103573>
- Rosen, D.E. and Patterson, C. 1969. The structure and relationships of the paracanthopterygian fishes. *American Museum of Natural History Bulletin*, 141:3.
- Ross, A.J. and Cook, E. 1995. The stratigraphy and palaeontology of the Upper Weald Clay (Barremian) at Smokejacks Brickworks, Ockley, Surrey, England. *Cretaceous Research* 16:705–716.
<https://doi.org/10.1006/cres.1995.1044>
- Rouillon, M. and Taylor, M.P. 2016. Can field portable X-ray fluorescence (pXRF) produce high quality data for application in environmental contamination research?. *Environmental Pollution*, 214:255–264.
<https://doi.org/10.1016/j.envpol.2016.03.055>
- Seilacher, A., Reif, W.E., Westphal, F., Riding, R., Clarkson, E.N.K., and Whittington, H.B. 1985. Sedimentological, Ecological and Temporal Patterns of Fossil Lagerstatten [and Discussion]. *Philosophical Transactions of the Royal Society B: Biological Sciences*, 311(1148):5–24.
<https://doi.org/10.1098/rstb.1985.0134>
- Toppe, J., Albrektsen, S., Hope, B., and Aksnes, A. 2007. Chemical composition, mineral content and amino acid and lipid profiles in bones from various fish species. *Comparative Biochemistry and Physiology Part B: Biochemistry and Molecular Biology*, 146(3):395–401.
<https://doi.org/10.1016/j.cbpb.2006.11.020>
- Varejão, F.G., Warren, L.V., Simões, M.G., Buatois, L.A., Mángano, M.G., Bahniuk Rumbelsgperger, A.M., and Assine, M.L. 2021. Mixed siliciclastic–carbonate sedimentation in an evolving epicontinental sea: Aptian record of marginal marine settings in the interior basins of north-eastern Brazil. *Sedimentology*, 68:2125–2164.
<https://doi.org/10.1111/sed.12846>
- Wang, L., Hu, D., Zhang, L., Zheng, S., He, H.Y., Deng, C., Wang, X.L., Zhou, Z.H., and Zhu, R.X. 2013. SIMS U-Pb zircon age of Jurassic sediments in Linglongta, Jianchang, western Liaoning, p. constraint on the age of the oldest feathered dinosaurs. *Chinese Science Bulletin*, 58(14):1346–1353.

APPENDIX 1.

APPENDIX TABLE 1. Extended information from each site, their location, age and some additional data and the principal references. Also are shown the sample name of this work to facilitate the acronym navigation in the paper.

Site Name	Location	Age	Lithology/Facies/ Formations	Description	Samples	References
Pedrera de Meià & Co.	Montsec de Meià, Spain	Upper Hauterivian - Barremian	Laminated and massive lithographic limestones.	19th century lithographic quarry. Limestones result of fresh-water coastal lakes system sedimentation of small extension.	R, R-drk, R-wht, C	Barale et al., 1984; Gil- Delgado et al., 2023; Martínez-Delclòs et al., 1991; Martín-Closas & López-Morón, 1995.
Alcover	Tarragona, Spain	Triassic	Dolomiticrites and dolomites from the Upper Muschelkalk.	Thin-bedded and laminated dolostones result of the infill of inter-reef depressions in anoxic conditions.	Mnt-Alc	Calvet & Tucker, 1995.
Rubielos de Mora	Rubielos de Mora, Spain	Miocene - Early Pliocene	Laminated and massive mudstones of delta and lake facies.	Marls and mudstones of transitional facies that forms a tertiary basin of variably 400 m thick.	RMr	Anadón, 1983; Anadón et al. 1988; Moissenet and Gautier, 1971.
Las Hoyas	Cuenca, Spain	Barremian	Finely-laminated limestones of La Huérguina Formation.	Limestones formed in a ponds of microbial mats bottom. Is a freshwater carbonate environment influenced by season regulation.	LH1, LH2	Bailleul et al., 2011; Barrios-de Pedro et al., 2018; Briggs et al., 1997; Fregenal and Meléndez, 1992; Fregenal-Martínez and Meléndez 2016; Galobart et al., 2022; Gupta et al., 2008; Poyato-Ariza and Buscalioni, 2016.
Cerin	Cerin, France	Late Kimmeridgian	Lithographic limestones.	Result of lagoon system in- filled with the action of supra-, intertidal, phreatic features and microbial processes.	Crn	Bernier et al., 1994.
Canjuers	Haute Provence (Les Bessons), France	Tithonian	Fine-layered lithographic limestones from lagoon facies.	The fossils are situated in the basal layers of these paleolagoon and corresponds to the first phase of sedimentation.	MCFO- 0352	Peyer et al., 2014.

Site Name	Location	Age	Lithology/Facies/ Formations	Description	Samples	References
Les Plâtrières	Aix-en-Provence, France	Oligocene	Limestones, marls and gypsum from Aix-en-Provence formation.	18th century quarry of laminated rocks, result of a lacustrine/lagoon environment of brackish waters with punctual sea connections.	Aix-P1, Aix-P2, Aix-P3	Gaudant et al., 2017.
Ockley (Smokejacks Brickworks)	Surrey, England	Early Barremian	Sideritic siltstone and mudstone lenses below sandstone-bed of the Upper Weald Clay.	Industrial exploitation in a changing sequence from a lacustrine/lagoonal to fluvial/mudplain environment (<i>B. walken</i> site from).	Ock	Ross & Cook, 1995.
Solnhofen	Solnhofen-Eichstätt, Germany	Early Tithonian	Lithographic limestones rhythmically laminated, alternation of pure limestone (Flinze) and shaly calcareous marls (Fäulen).	The Bavarian sites pertains to the Solnhofen Plattenkalk, which occupies an area of more than 2000 km ² and records 500.000 years.	MCFO-0435, MCFO-0723b, MCFO-0528, MCFO-0530, MCFO-	Keupp et al. 2007.
Kelheim	Kelheim, Germany	Tithonian	Alternation of Flinze (97-99% CaCO ₃) and Fäulen (80-90% CaCO ₃).	The formation of Solnhofen Plattenkalk starts at east of the Solnhofen town and prograde to west during Early Tithonian. Is the reason because there are very similar fossil sites in the zone, as Kelheim, at 150 kilometers at east.	MCFO-0436	Keupp et al. 2007.
Hakel	east of Jbail, Lebanon	Late Cenomanian	Lithographic limestones.	Sites are interpreted as small basins of shallow waters like intra-shelf depressed zones. There appears carbonates of shallow-waters between laminated mudstones as a result of sea-level oscillations.	MCFO-0521, MCFO-0523	Ejel and Dubertret, 1966; Ferry et al., 2007; Forey et al., 2003.
Hadjoula	east of Jbail, Lebanon	Late Cenomanian	Lithographic limestones.	"	MCFO-0372, MCFO-0527, MCFO-	Ejel and Dubertret, 1966; Ferry et al., 2007; Forey et al., 2003.
Sahel Alma	south of Jbail, Lebanon	Late Santonian	Fine-grained, chalky limestones that broke in slabs.	Fossil site deposits are from deeper Santonian waters.	MCFO-0520	Jattiot et al., 2015; Meister, 1993.

Site Name	Location	Age	Lithology/Facies/ Formations	Description	Samples	References
Karatau	Big Karatau Range, Kazakhstan	Callovian - Kimmeridgian / Oxfordian - Kimmeridgian	Lithographic shales in Karabatau Formation.	The fossil site is composed by very laminated fissile claystone of lacustrine deposits that can preserve soft parts of taxa.	Kr	Doludenko and Orlovskaia, 1976; Doludenko et al., 1990; Liu et al., 2015.
Daohugou	Daohugou, China	Callovian - Oxfordian	Grey tuff, tuffaceous siltstone and mudstone situated in Daohugou Beds of Langi Formation.	The fossils are preserved in the mudstones among fresh water environment indicators. Is the most important Lagerstätte of insects from Mesozoic.	Dhg	Liu et al., 2015; Ponomarenko and Ren, 2010; Rasnitsyn and Zhang, 2004; Wang et al., 2013.
Green River	Wyoming, USA	Early Eocene - Middle Eocene	Laminated calcite limestone, limestones, marlstones and iron-stained mudstones principally .	Lake system with different basins and all their facies. In general terms, in Wyoming there are two paleolakes represented, the Fossil Lake and Lake Gosiute.	MCFO-0143, MCFO-0395	Grande, 1984; Lundberg and Case, 1970; Rosen and Patterson, 1969.
Crato	Crato, Brazil	Aptian	Laminated limestones of microbial mats in Crato Formation of lacustrine facies.	Site generated by the carbonate deposition in a hypersaline lacustrine system emplaced on the basin associated with the Gondwana rifting, considered a wetland with seasonal changes.	Crt-BrsI	Arai and Assine, 2020; Brito Neves et al., 2000; Dias and Carvalho, 2022; Ribeiro et al., 2021; Varejao et al., 2021.

APPENDIX TABLE 2. Intensity of the main XRF peaks detected for all the samples investigated in this work. The intensities were extracted by fitting the spectra as described in (Ibáñez-Lhsa, 2017). All intensity values are normalized to that of the Compton peak observed for each spectra.

SAMPLE	ID	Si	P	S	K	Ca	Ti	Cr	Fe	Cu	Zn	Pb	Rb	Sr	Zr
MCFO-0143	Green River	0.0040	0.0398	0.0134	0.0098	3.6275	0.0023	0.0012	0.0521	0.0057	0.0064	0.0107	0.0000	0.7690	0.0322
MCFO-0143	Green River F	0.0017	0.0435	0.0094	0.0091	2.4378	0.0561	0.0010	0.2545	0.0107	0.0140	0.0090	0.0000	1.5172	0.0115
MCFO-0435	Solnhofen	0.0035	0.0439	0.0154	0.0376	4.0263	0.0068	0.0020	0.1745	0.0047	0.0091	0.0085	0.0000	0.1193	0.0070
MCFO-0436	Kelheim	0.0015	0.0309	0.0073	0.0467	2.4534	0.0144	0.0016	0.8939	0.0045	0.0068	0.0065	0.0143	0.2154	0.0107
MCFO-0436	Kelheim	0.0019	0.0269	0.0059	0.0484	2.3883	0.0147	0.0014	0.8573	0.0041	0.0084	0.0037	0.0084	0.2090	0.0126
MCFO-0723b	Solnhofen	0.0020	0.0444	0.0059	0.0262	4.1467	0.0029	0.0017	0.1269	0.0051	0.0056	0.0034	0.0000	0.0827	0.0069
MCFO-0527	Hjoula	0.0122	0.0088	0.0048	0.0054	0.1822	0.0037	0.0006	0.0818	0.0031	0.0048	0.0019	0.0000	0.0394	0.0090
MCFO-0527	Hjoula	0.0003	0.0357	0.0082	0.0310	3.4217	0.0046	0.0006	0.0903	0.0050	0.0071	0.0019	0.0000	0.2205	0.0042
MCFO-0521	Haqel	0.0022	0.0335	0.0080	0.0433	2.6311	0.0115	0.0011	0.2634	0.0046	0.0068	0.0077	0.0000	0.4253	0.0113
MCFO-0528	Solnhofen	0.0000	0.0450	0.0107	0.0277	3.8885	0.0036	0.0013	0.2137	0.0060	0.0040	0.0053	0.0000	0.1326	0.0078
MCFO-0527	Hjoula	0.0013	0.0356	0.0092	0.0347	3.4503	0.2378	0.0005	0.1564	0.0062	0.0071	0.0038	0.0000	0.2452	0.0152
MCFO-0530	Solnhofen	0.0022	0.0451	0.0118	0.0268	3.8685	0.0067	0.0010	0.1968	0.0056	0.0040	0.0035	0.0000	0.1306	0.0104
MCFO-0522	Hjoula	0.0014	0.0360	0.0129	0.0355	3.1842	0.0067	0.0006	0.2252	0.0052	0.0052	0.0033	0.0000	0.3644	0.0159
MCFO-0352	Haute-Provence	0.0018	0.0164	0.0069	0.0309	1.4130	0.0130	0.0011	0.6059	0.0083	0.0086	0.0046	0.0031	0.5530	0.0027
MCFO-0395	Green River	0.0024	0.0352	0.0115	0.0296	3.6251	0.0019	0.0014	0.0520	0.0085	0.0054	0.0067	0.0000	0.6383	0.0085
MCFO-0520	Sahel Alma	0.0017	0.0340	0.0062	0.0423	2.7029	0.0081	0.0019	0.2853	0.0062	0.0104	0.0089	0.0000	0.4291	0.0145
MCFO-0524	Hjoula	0.0033	0.0341	0.0080	0.0304	3.1934	0.0050	0.0009	0.1357	0.0048	0.0081	0.0081	0.0000	0.4126	0.0192
MCFO-0525	Hjoula	0.0036	0.0314	0.0084	0.0354	2.8704	0.0081	0.0011	0.2655	0.0056	0.0104	0.0071	0.0000	0.3288	0.0096
MCFO-0523	Haqel	0.0035	0.0288	0.0085	0.0403	2.9374	0.0066	0.0016	0.2329	0.0051	0.0088	0.0052	0.0000	0.4494	0.0083
MCFO-0526	Solnhofen	0.0022	0.0391	0.0115	0.0222	4.0393	0.0043	0.0008	0.1237	0.0035	0.0058	0.0053	0.0000	0.2268	0.0054
R-drk	Montsec	0.0029	0.0353	0.0106	0.0227	3.7724	0.0071	0.0005	0.1867	0.0046	0.0057	0.0054	0.0000	0.1678	0.0103
R-wht	Montsec	0.0032	0.0380	0.0102	0.0300	3.7859	0.0128	0.0015	0.3440	0.0049	0.0052	0.0046	0.0000	0.1211	0.0052
C	Montsec	0.0015	0.0388	0.0137	0.0208	4.0036	0.0049	0.0003	0.1698	0.0044	0.0061	0.0051	0.0000	0.1453	0.0041
LH1	Las Hoyas	0.0016	0.0376	0.0166	0.0196	3.4479	0.0079	0.0012	0.2988	0.0041	0.0092	0.0047	0.0000	0.6435	0.0125
LH2	Las Hoyas	0.0015	0.0390	0.0155	0.0167	3.5759	0.0047	0.0017	0.2196	0.0062	0.0067	0.0082	0.0000	0.7874	0.0109
MGB PR-10378	Solnhofen	0.0009	0.0430	0.0196	0.0070	4.3715	0.0011	0.0012	0.0304	0.0069	0.0069	0.0145	0.0000	0.2242	0.0185
MGB PR-10347	Solnhofen	0.0003	0.0474	0.0140	0.0132	4.2524	0.0023	0.0014	0.0826	0.0057	0.0061	0.0301	0.0000	0.2181	0.0218
paraloid 10%	Montsec	0.0003	0.0342	0.0093	0.0161	3.2536	0.0079	0.0008	0.1865	0.0066	0.0060	0.0080	0.0000	0.1333	0.0049
paraloid 5%	Montsec	0.0016	0.0341	0.0090	0.0180	3.4406	0.0105	0.0010	0.2283	0.0039	0.0049	0.0070	0.0000	0.1358	0.0046
paraloid 0%	Montsec	0.0021	0.0445	0.0099	0.0145	4.1477	0.0060	0.0007	0.1299	0.0039	0.0044	0.0053	0.0000	0.1355	0.0139
Crn	Cerin	0.0000	0.0401	0.0126	0.0061	3.8339	0.0046	0.0012	0.0305	0.0042	0.0024	0.0066	0.0000	0.1043	0.0080
Kr	Karatu	0.0008	0.0172	0.0062	0.0095	1.1201	0.0151	0.0024	0.9903	0.0053	0.0036	0.0119	0.0065	1.5199	0.0390
Mnt-Alc	MontRai-Alcover	0.0086	0.0058	0.0042	0.0324	0.5287	0.0353	0.0032	0.5737	0.0066	0.0025	0.0052	0.0012	0.2251	0.0122
Ock	Ockley	0.0060	0.0040	0.0008	0.0774	0.0839	0.2013	0.0348	14.8936	0.0066	0.0138	0.0112	0.0604	0.0536	0.0144
Ock	Ockley	0.0080	0.0040	0.0001	0.0808	0.0849	0.2028	0.0359	15.7104	0.0093	0.0146	0.0107	0.0618	0.0564	0.0213
RMr	Rubielos de Mora	0.0026	0.0077	0.0058	0.0618	0.7595	0.0286	0.0050	1.3111	0.0060	0.0100	0.0097	0.0812	0.3793	0.0110
Dhg	Daohugou	0.0064	0.0036	0.0035	0.0430	0.0338	0.0159	0.0021	0.7439	0.0031	0.0070	0.0061	0.0859	0.0881	0.0261

SAMPLE	ID	Si	P	S	K	Ca	Ti	Cr	Fe	Cu	Zn	Pb	Rb	Sr	Zr
Slnhf-1	Solnhofen	0.0119	0.0201	0.0053	0.0038	1.7998	0.0027	0.0007	0.0257	0.0033	0.0117	0.0113	0.0000	0.0823	0.0051
Slnhf-2	Solnhofen	0.0059	0.0162	0.0059	0.0086	1.5040	0.0053	0.0007	0.2299	0.0062	0.0097	0.0039	0.0000	0.0502	0.0066
Crt-Brsl	Crato	0.0017	0.0460	0.0138	0.0103	4.0442	0.0035	0.0012	0.4043	0.0072	0.0395	0.0101	0.0000	0.5558	0.0031
Aix-P1	Aix-en-Provence	0.0054	0.0295	0.0146	0.0107	2.6703	0.0034	0.0008	0.1194	0.0057	0.0049	0.0083	0.0000	3.2992	0.0204
Aix-P2	Aix-en-Provence	0.0068	0.0060	0.0037	0.0101	0.6566	0.0040	0.0007	0.1401	0.0024	0.0017	0.0028	0.0000	0.1710	0.0036
Aix-P3	Aix-en-Provence	0.0088	0.0190	0.0075	0.0227	2.0929	0.0054	0.0004	0.2497	0.0034	0.0034	0.0052	0.0000	0.2797	0.0073